We are IntechOpen,
the world's leading publisher of
Open Access books
Built by scientists, for scientists

6,900
Open access books available

186,000
International authors and editors

200M
Downloads

Our authors are among the

154
Countries delivered to

TOP 1%
most cited scientists

12.2%
Contributors from top 500 universities

CLARIVATE ANALYTICS
BOOK CITATION INDEX
INDEXED

WEB OF SCIENCE™

Selection of our books indexed in the Book Citation Index
in Web of Science™ Core Collection (BKCI)

Interested in publishing with us?
Contact book.department@intechopen.com

Chapter

Dielectric Responses in Multilayer C$_f$/Si$_3$N$_4$ as High-Temperature Microwave-Absorbing Materials

Heng Luo, Lianwen Deng and Peng Xiao

Abstract

High-temperature microwave-absorbing materials are in great demand in military and aerospace vehicles. The high-temperature dielectric behavior of multilayer C$_f$/Si$_3$N$_4$ composites fabricated by gelcasting has been intensively investigated at temperature coverage up to 800°C in the X-band (8.2–12.4 GHz). Experimental results show that the permittivity of Si$_3$N$_4$ matrix exhibits excellent thermo-stability with temperature coefficient lower than 10^{-3}°C^{-1}. Taking temperature-dependent polarized bound charge and damping coefficient into consideration, a revised dielectric relaxation model with Lorentz correction for Si$_3$N$_4$ ceramics has been established and validated by experimental results. Besides, a general model with respect to permittivity as a function of temperature and frequency has been established with the help of nonlinear numerical analysis to reveal mechanisms of temperature-dependent dielectric responses in C$_f$/Si$_3$N$_4$ composites. Temperature-dependent permittivity has been demonstrated to be well distributed on circular arcs with centers actually kept around the real (ε') axis in the Cole-Cole plane. Furthermore, space charge polarization and relaxation are discussed. These findings point to important guidelines to reveal the mechanism of dielectric behavior for carbon fiber functionalized composites including but not limited to C$_f$/Si$_3$N$_4$ composites at high temperatures, and pave the way for the development of high-temperature radar absorbing materials.

Keywords: high temperature, microwave-absorbing material, dielectric, relaxation

1. Introduction

Wireless electronic devices and communication instruments have found wide application in our daily life. Their efficient operation depends strongly on transmission behavior of alternating electromagnetic wave with frequency ranging from kilohertz (KHz) to gigahertz (GHz), and vice versa, are very sensitive to interference from external electromagnetic wave. Driven by the demand for both adequate interference rejection and controlled radiation, more and more efforts have been devoted to high-performance electromagnetic compatibility/interference (EMC/EMI) materials. As we all know, the propagation behavior of electromagnetic wave when encountering a material could be divided into three types in principle: reflection, absorption, and transmission. As typical EMI materials, metals or materials with high electrical conductivity could prevent external electromagnetic wave from

penetration due to the large amount of free electrons. Last decades have witnessed intensive efforts toward exploring lightweight and cost-effective electromagnetic interference (EMI) materials with adequate shielding effectiveness [1–5], involving carbonaceous fillers-enabled polymers, novel lightweight metal composites, etc.

However, the primary function of EMI shielding is to reflect radiation using charge carriers that interact directly with incident electromagnetic field, and the back-radiation would in turn affect the surrounding environment and devices. What is more, the reflected radiation may also be caught by radar observation systems and lead to exposure of moving trace, which is extremely undesirable from the defense-oriented point of view. As a result, electromagnetic wave-absorbing materials with reduced reflection on the surface as well as enhanced internal attenuation are more favorable candidates for EMI shielding, especially in the GHz range. Polymers modified by carbon nanomaterials (e.g., carbon nanotubes [6–8], carbon nanofibers [9, 10], graphene [11, 12], etc.), metal powders [13, 14], and ferrite [15] have been demonstrated to be excellent microwave-absorbing/ shielding materials especially in the X-band (8.2–12.4 GHz) [16, 17], and have achieved successful application [18–20]. However, due to their inferior temperature stability and mechanical properties, their application is limited toward application under high temperature. For example, the temperature on the windward side of high-speed aircraft (>3 Ma) could reach up to 1000°C due to the aerodynamic heating effect. As a result, ceramics and their derivative architecture (r-GOs/SiO$_2$, CNT/SiO$_2$, ZnO/ZrSiO$_4$, SiC$_f$/SiC, etc.) [21–30] with the integration of desirable dielectric responses, high strength, oxidation resistance, thermo-stability, and low density have attracted growing attention for high-temperature-absorbing materials. Besides, Si$_3$N$_4$ ceramics are one of the most intensively studied ceramics in high-temperature applications due to their superior antioxidation (>1200°C) and mechanical and chemical stabilization properties [31–38]. More importantly, owing to the excellent electrical insulation property and low dielectric constant, Si$_3$N$_4$ ceramics are expected to be a promising candidate matrix as high-temperature microwave-absorbing materials [25, 29, 30, 39–42]. However, previous work mainly focused on experimental evolution of complex dielectric responses with temperature and qualitative analyses according to the Debye theory. Still, modeling for high-temperature dielectric behaviors is relatively limited and remains a great challenge due to the complexity of the components and microstructures for high-temperature microwave-absorbing materials, as well as high-temperature measurement system. It also should be noted that microwave dissipation capacity of a composite is strongly dependent on the structural design. Many investigations have shown that incorporation of reasonable structural design, involving multilayer structure [43–45] and periodic structure in metamaterials [46, 47], is an effective way to regulate dielectric response and guarantee desirable attenuation performance. Moreover, taking full advantage of tunable electromagnetic parameters in each layer, optimal microwave impedance matching as well as absorbing capability could be achieved. This fact means that it is essential to explore the mechanism of dielectric behavior of laminate-structure materials from new viewpoints.

In this chapter, we mainly focus on the microwave dielectric responses in laminate-structure or multilayer-structure C$_f$/Si$_3$N$_4$ composites from both experimental and theoretical points of view. Furthermore, a general model with respect to permittivity as a function of temperature and frequency would be established to reveal mechanisms of temperature-dependent dielectric responses for C$_f$/Si$_3$N$_4$ composites. These findings point to important guidelines to reveal the mechanism of dielectric behavior for carbon fiber functionalized composites including but not limited to C$_f$/Si$_3$N$_4$ composites at high temperatures, and pave the way for the development of high-temperature radar absorbing materials.

2. Experiments

2.1 Preparation of multilayer C$_f$/Si$_3$N$_4$ composites

Commercially available carbon fibers (T700, 12 K, TohoTenax Inc., Japan) were used as starting materials in this work. In order to avoid damage at high-temperature sintering, pyrolytic carbon(PyC)/SiC dual-coating on carbon fibers was prepared by chemical vapor deposition based on Methyltrichlorosilane (MTS)-H2-Ar system at 1150°C. The powder mixture of 85 wt% α-Si$_3$N$_4$ (purity > 93%, d$_{50}$ = 0.5 μm, Beijing Unisplendor Founder High Technology Ceramics Co. Ltd., China), 5 wt% Al$_2$O$_3$, and 10 wt% Y$_2$O$_3$ was mixed with solvent-based acrylamide-N,N′-methylenebisacrylamide (AM-MBAM) system, and consolidated via gelcasting and pressureless-sintering route (as illustrated in **Figure 1**). Details of the multilayer C$_f$/Si$_3$N$_4$ samples' preparation are given in our previous work [35]. Note that each layer of carbon fiber plays dominant role to attenuate microwave energy, which could be adjudged the surface density of short carbon fiber.

2.2 High-temperature electromagnetic measurements

In order to evaluate the high-temperature permittivity, specimens with the size of 22.86 × 10.16 × 1.5 mm^3 were polished and determined in X-band through the wave-guide method with a vector network analyzer (Agilent N5230A, USA). As shown in **Figure 2**, the as-prepared Si$_3$N$_4$ ceramic sample was heated by an inner heater with a ramp rate of 10°C/min up to 800°C in air. For accuracy of measurement, the device was carefully calibrated with the through-reflect-line (TRL) approach, and a period of 10 min was applied to guarantee system stability at each evaluated temperature.
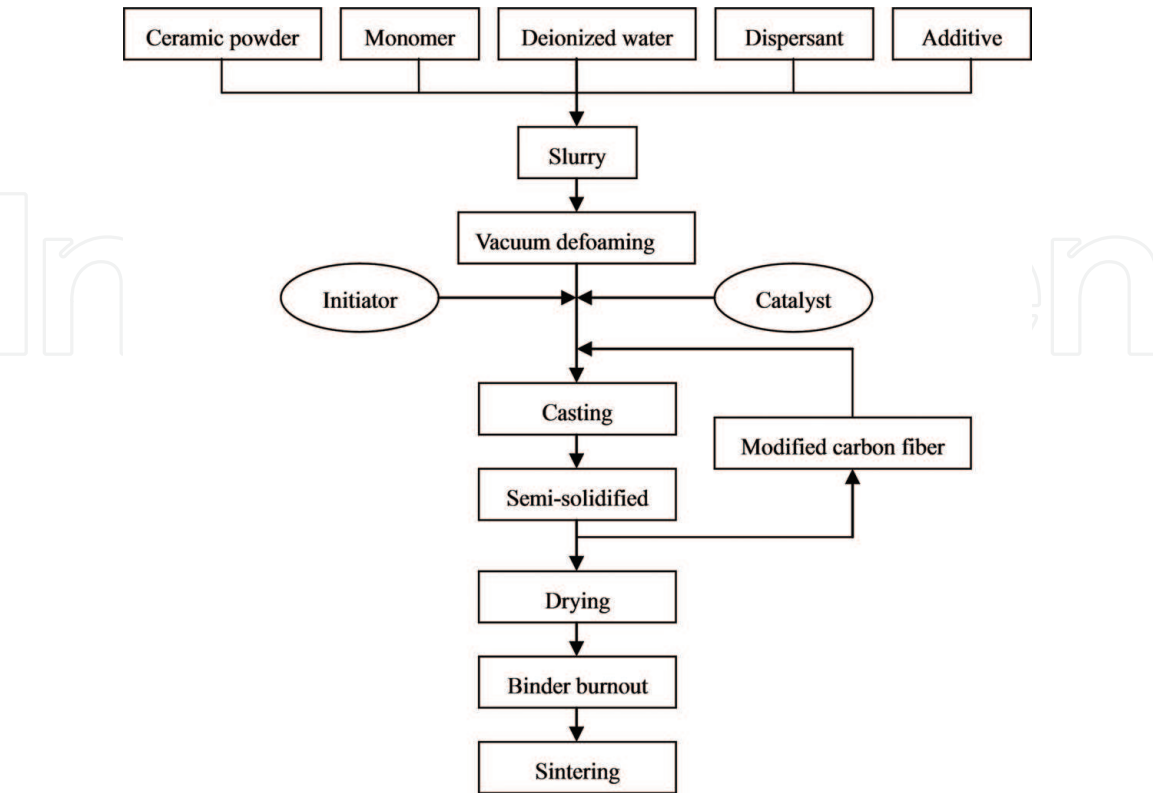
Figure 1.
The gelcasting process for preparation of multilayer C$_f$/Si$_3$N$_4$ composites (reprinted with permission from Ref. [35]).

Figure 2.
Schematic diagram of complex permittivity test apparatus (reprinted with permission from Ref. [48]).
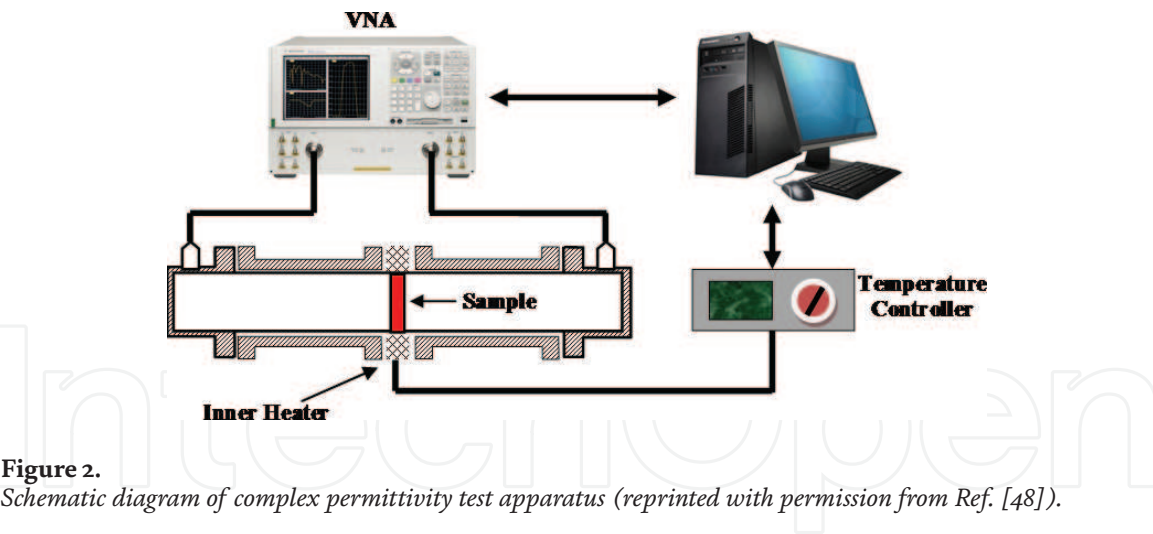
3. Microwave dielectric properties

3.1 Structure of multilayer C_f/Si_3N_4 composites

The optical image of cross-section of multilayer C_f/Si_3N_4 composites is shown in **Figure 3(a)**. As expected, three layers filled with short carbon fibers are uniformly embedded in the Si_3N_4 matrix. The microstructure of Si_3N_4 ceramic was formed by rod-like particles, which are evenly distributed and intercross with each other to form the main pores. Energy dispersive spectroscopy (EDS) analysis at spots A and B in **Figure 3(c)** demonstrates that the PyC/SiC interphase could effectively promote the chemical compatibility between carbon fibers and Si_3N_4 ceramic at high-temperature circumstance, which could be further proved by the XRD investigations (see **Figure 4**). As seen in **Figure 4**, in addition to the main β-Si_3N_4 peaks
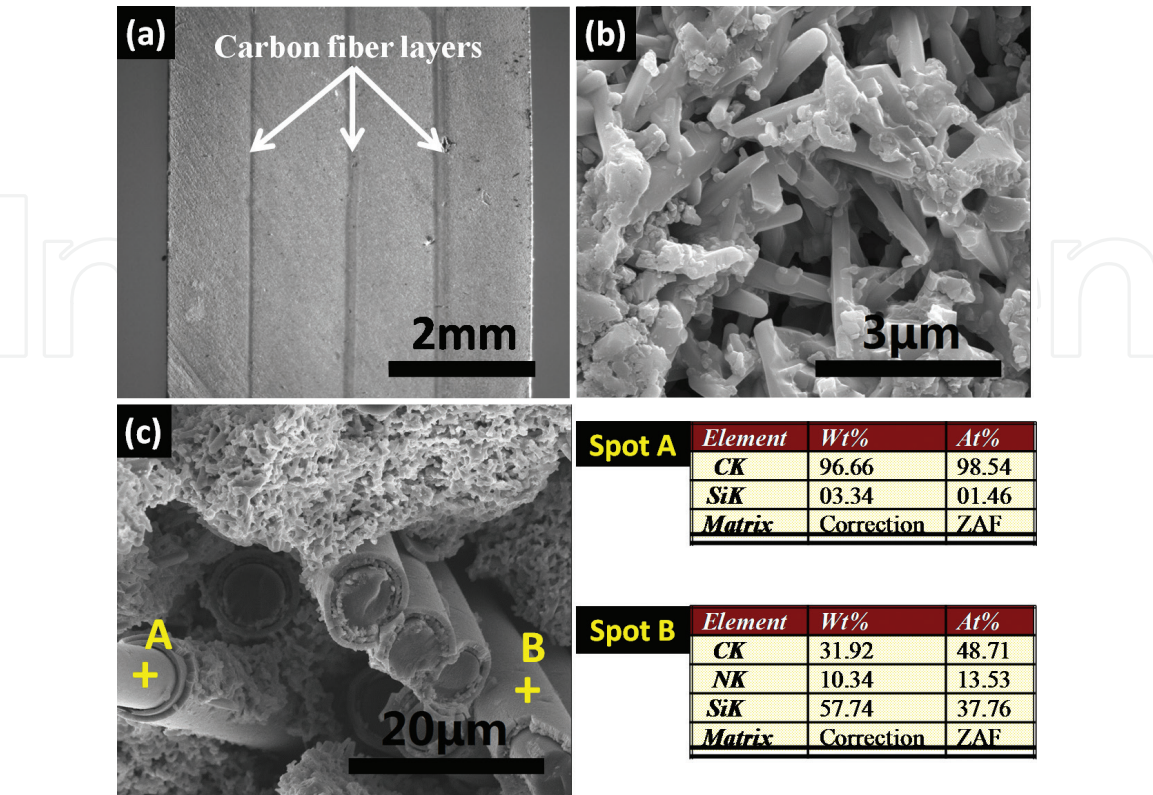

Spot A	Element	Wt%	At%
	CK	96.66	98.54
	SiK	03.34	01.46
	Matrix	Correction	ZAF

Spot B	Element	Wt%	At%
	CK	31.92	48.71
	NK	10.34	13.53
	SiK	57.74	37.76
	Matrix	Correction	ZAF

Figure 3.
(a) Cross-section of multilayer C_f/Si_3N_4 composites, facture surface located at (b) Si_3N_4 matrix and (c) carbon fibers (reprinted with permission from Ref. [39]).

and Y-Al oxide peaks, additional C and β-SiC peaks, corresponding to the carbon fiber and modification coating, were detected for C$_f$/Si$_3$N$_4$ composites.

3.2 Room-temperature dielectric properties of multilayer C$_f$/Si$_3$N$_4$ composites

According to the classical transmission line theory, microwave complex permittivity ($\varepsilon = \varepsilon' - j\varepsilon''$) is an important parameter to determine the absorbing performance. **Figure 5(a)** shows the real and imaginary permittivity of multilayer C$_f$/Si$_3$N$_4$ composites at X-band, as well as as-prepared Si$_3$N$_4$ ceramics. Clearly, the dielectric constant of Si$_3$N$_4$ ceramics presents frequency-independent behavior. The mean real and imaginary parts of permittivity and dielectric loss ($\tan\delta = \varepsilon''/\varepsilon'$) of pure Si$_3N_4$ ceramic were 7.7, 0.04, and 5.3×10^{-3}, respectively. The relatively low dielectric constant is considered to be helpful for microwave impedance matching with free space, which tends to reduce reflection of electromagnetic wave from the surface of material and enhance energy propagating in the material.

However, both the real permittivity and imaginary permittivity of C$_f$/Si$_3$N$_4$ sandwich composites decrease markedly as frequency increases at X-band, varying from 12.3 and 5.1 to 7.9 and 1.2, respectively. This phenomenon is usually called frequency dispersion characteristic, which is acknowledged to be beneficial to broaden the microwave absorption bandwidth. The reflection loss (R) of Si$_3$N$_4$ and C$_f$/Si$_3$N$_4$ sandwich composites was calculated according to the formula as follows:

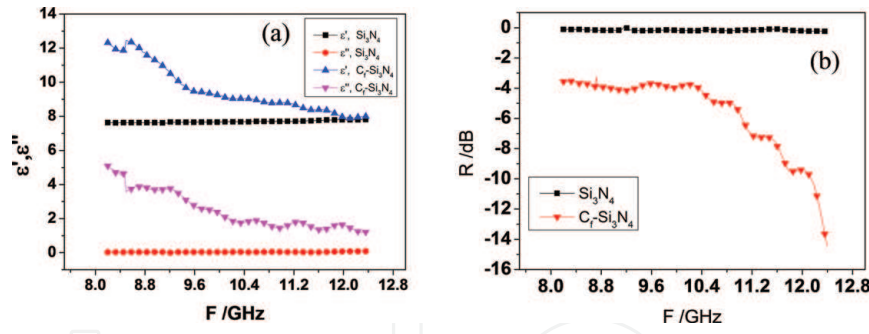$$R(dB) = 20 \log\left|\frac{Z_{in} - 1}{Z_{in} + 1}\right| \tag{1}$$

and

$$Z_{in} = \sqrt{\frac{\mu_r}{\varepsilon_r}} \tanh\left[j\left(\frac{2\pi}{c}\right)\sqrt{\mu_r \varepsilon_r} fd\right] \tag{2}$$

where Z_{in} refers to input impedance, j is the imaginary unit (i.e., equals to $\sqrt{-1}$), c is the velocity of electromagnetic waves in free space, f is the microwave frequency,
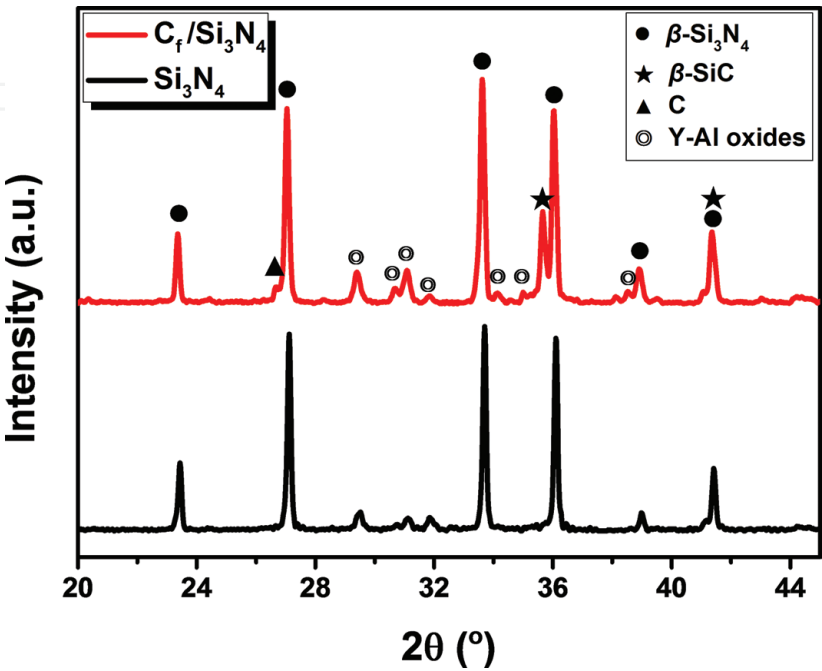
Figure 4.
XRD patterns of as-prepared Si$_3$N$_4$ ceramics and C$_f$/Si$_3$N$_4$ composites (reprinted with permission from Ref. [39]).

Figure 5.
(a) The permittivity and (b) reflection loss curves of Si$_3$N$_4$ and C$_f$/Si$_3$N$_4$ sandwich composites over X-band (reprinted with permission from Ref. [35]).

and *d* is the thickness of the samples. As depicted in **Figure 5(b)**, the microwave absorption ability of the C$_f$/Si$_3$N$_4$ sandwich composites was significantly enhanced compared with pure Si$_3$N$_4$ ceramic. The reflection loss of the C$_f$/Si$_3$N$_4$ sandwich composites gradually decreases from −3.5 dB to −14.4 dB with the increase of frequency, while that of the pure Si$_3$N$_4$ ceramic remains at −0.1 dB.

The enhanced microwave-absorbing performance could be mainly attributed to polarization relaxation. As we know, there exists migration of free electrons inside the electro-conductive carbon fibers, as well as charge accumulation at interfaces between short carbon fibers and insulated matrix when subjected to external electric field. As a result, the chopped carbon fibers are more inclined to be equivalent to micro-dipoles. With increase of frequency, the orientation of these dipoles could not keep up with change of electric field gradually, resulting in the real part of permittivity (ε') of C$_f$/Si$_3$N$_4$ sandwich composites decrease gradually. Furthermore, the scattering effect from defects and the crystal lattice on the back-and-forth movement of electrons under alternating electromagnetic waves predominately contributes to the dissipation of EM energy, which results in thermal energy.

For a deep-seated investigation of frequency-dependent dielectric responses of multilayer C$_f$/Si$_3$N$_4$ composites (**Figure 6(a)**), here we proposed an equivalent RC circuit model, where each layer of carbon fiber plays a role of one electrode in a plane-parallel capacitor, while each layer of Si$_3$N$_4$ ceramic plays the role of the dielectric (**Figure 6(b)**). Considering the existence of leakage current, leakage resistances were applied in equivalent circuit (**Figure 6(c)**).

According to the circuit theory knowledge, the relationship between permittivity and frequency ω follows:

$$\varepsilon' = \frac{Q(C_1 + C_2)^2}{R_1^2 C_1 C_2 (C_1 + C_2)} \cdot \frac{1}{\omega^2} + \frac{Q R_1^2 C_1^2 C_2^2}{R_1^2 C_1 C_2 (C_1 + C_2)}$$

$$\omega \cdot \varepsilon'' = P \frac{(C_1 + C_2)^2 + R_1^2 C_1^2 C_2^2 \cdot \omega^2}{(R_1 + R_2)(C_1 + C_2)^2 + R_1^2 R_2 C_1^2 C_2^2 \cdot \omega^2} \tag{3}$$

where *P*, *Q*, and *C* are constants and are determined by the surface density of carbon fiber layers and thickness of Si$_3$N$_4$ layers. We have analyzed our experimental permittivity based on Eq. (3) using Trust-Region algorithm, which is illustrated in **Figure 7**. The points in **Figure 7** indicate the experimental data, while the results predicted by equivalent circuit model are given as solid line. Clearly, for multilayer C$_f$/Si$_3$N$_4$ composites, both ε' and ($\omega \cdot \varepsilon''$) are inversely proportional to the frequency square ω^2, and the predicted results agree quite well with the measured data. Additionally, the experimental data show oscillation phenomena at high frequency, which may result from charge and discharge processes between C$_1$ and C$_2$ (**Figure 6**) with the increase of frequency. Note that, even though the imaginary part of
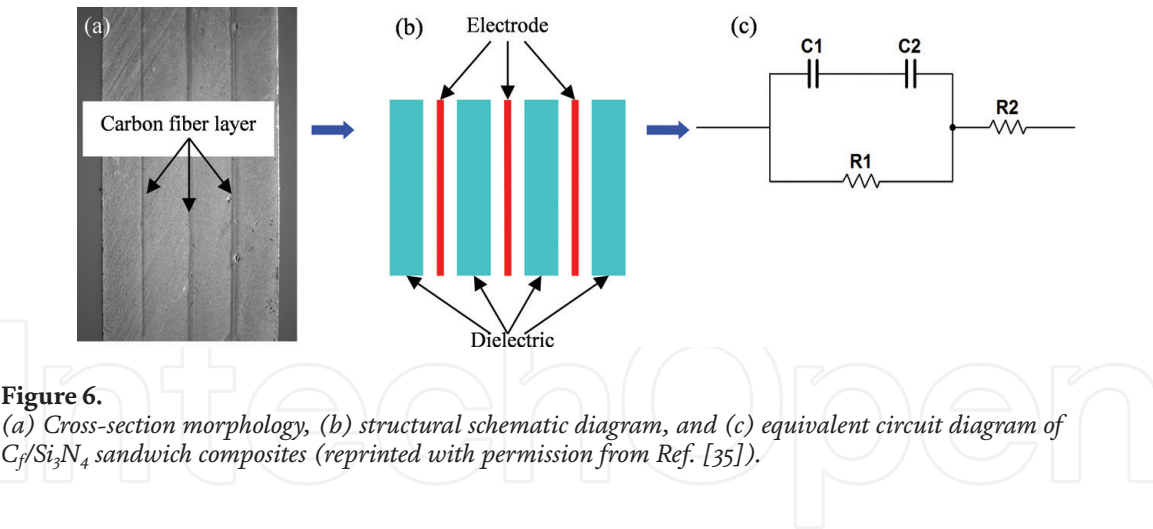
Figure 6.
(a) Cross-section morphology, (b) structural schematic diagram, and (c) equivalent circuit diagram of C$_f$/Si$_3$N$_4$ sandwich composites (reprinted with permission from Ref. [35]).
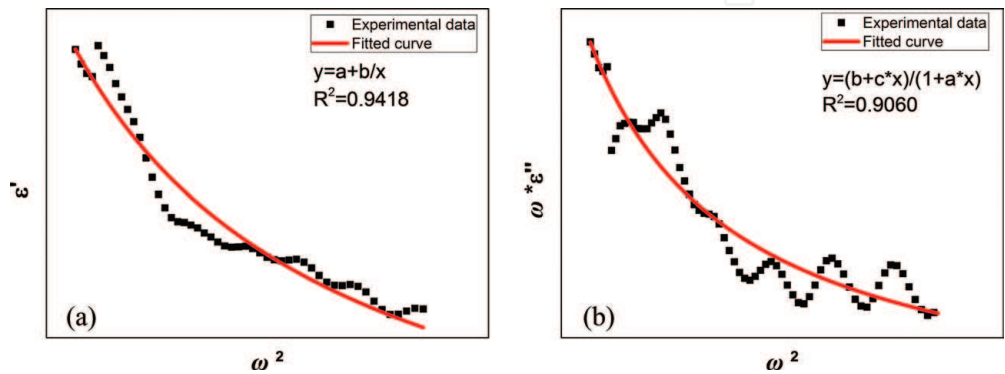
Figure 7.
Experimental data and curves of (a) ε′ and (b) ω·ε″ versus ω2 (reprinted with permission from Ref. [35]).

permittivity declines faster than the real part with frequency increase, the reflection loss presents enhanced trend with frequency increase. This phenomenon is mainly attributed to the fact that microwave-absorbing efficiency is the combination of reflection from the material surface and attenuation inside the material. The lower the permittivity, the better its impedance matching between air and absorber. As a result, in order to achieve optimal reflection loss, one must lower reflection as much as possible and keep a modest loss tangent simultaneously.

3.3 High-temperature dielectric behaviors of Si$_3$N$_4$ ceramics

Due to the fact that there will inevitably be some variation of electromagnetic performance or even the mechanical property of materials served in high-temperature condition, the dielectric property would be supposed to dynamically change with temperature. How and to what extent does the permittivity dynamically change with temperature (increase or decrease)? All these are quite critical in parameter modification strategy for improving the accuracy of radar detection and guidance. Consequently, it is of utmost importance to explore the evolution of dielectric properties of Si$_3$N$_4$ ceramics used in high-temperature circumstances. Three-dimensional (3D) plots of the effect of temperature on permittivity of Si$_3$N$_4$ ceramics over X-band are shown in **Figure 8**. Clearly, the real permittivity (ε′) shows no obvious change even though temperature rises up to 800°C. Likewise, thanks to the excellent electrical insulation of Si$_3$N$_4$ ceramics, the loss tangent (as shown in **Figure 8(b)**) is almost independent of frequency and temperature and remains lower than 0.06.

Herein, temperature coefficient κ is used to explicate the impact of temperature on dielectric response of as-prepared Si$_3$N$_4$ ceramics:
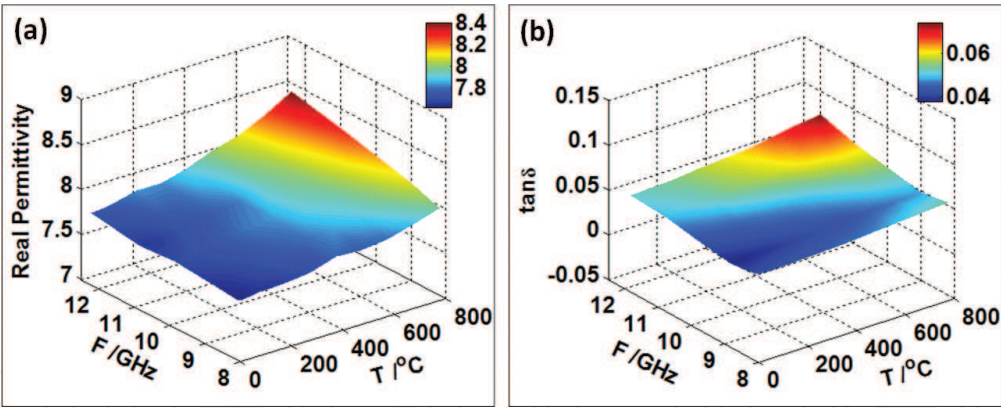
Figure 8.
Three-dimensional plots of complex permittivity of Si_3N_4 ceramics versus frequency and temperature (reprinted with permission from Ref. [39]).

$$\kappa = \frac{1}{\varphi} \cdot \frac{\Delta\varphi}{\Delta T}, \tag{4}$$

where T is the temperature and φ refers to either the dielectric constant or loss tangent. As summarized in **Table 1**, the temperature coefficients of both dielectric constant and loss tangent remain around $10^{-4\circ}C^{-1}$. From this perspective, the as-prepared Si_3N_4 ceramics exhibit excellent thermo-stability of dielectric response within the range of evaluated temperatures. This weak temperature dependence further corroborates as-prepared Si_3N_4 ceramics to be a competitive candidate as the matrix of high-temperature microwave-absorbing materials.

It should be noted that the real permittivity increases slightly with frequency increase, which is contrary to the ordinary frequency dispersion effect described by the Debye model [49–55]. In order to further expound this peculiar frequency dispersion characteristic, it is essential to explore the details of electronic polarizing processing of Si_3N_4 ceramics. Considering the covalent bonding, the electronic polarization in Si_3N_4 ceramics mainly results from the bound charge's displacement deviated from the equilibrium position. The motion equation of bound charge driven by an external electric field $E_0 e^{j\omega t}$ can be expressed as:

$$m\frac{\partial^2 x}{\partial t^2} = qE_0 e^{j\omega t} - fx - 2\eta\frac{\partial x}{\partial t} \tag{5}$$

Temperature (°C)	$\kappa_{\varepsilon'}$ ($\times 10^{-4\circ}C^{-1}$)		$\kappa_{\tan\delta}$ ($\times 10^{-4\circ}C^{-1}$)	
	8.2 GHz	12.4 GHz	8.2 GHz	12.4 GHz
25	0.46	0.45	2.08	2.84
100	0.22	0.93	1.79	3.11
200	0.45	0.031	2.83	4.83
300	1.04	1.02	3.02	3.91
400	0.16	1.31	2.87	4.89
500	0.40	1.11	4.98	6.92
600	0.97	1.70	4.68	5.97
700	1.16	1.94	3.49	4.34

Table 1.
Temperature coefficient of permittivity and loss tangent at selected frequency (reprinted with permission from Ref. [39]).

where m, q, and x are the mass, charge, and displacement of single bound charge, respectively; f is the coefficient of restoring force; and η is the damping coefficient. Taking Lorentz correction [56–58] into consideration, the real permittivity of Si$_3$N$_4$ ceramic containing N polarized bound charges could be obtained as:

$$\varepsilon = \varepsilon_s + \frac{Nq^2}{\varepsilon_0 m} \cdot \frac{\omega_0^2 - \omega^2}{\left(\omega_0^2 - \omega^2\right)^2 + 4\eta^2 \omega^2} \tag{6}$$

where ω_0 is the resonant frequency of Si$_3$N$_4$ ceramics, and ε_0 and ε_s are the vacuum permittivity and static dielectric constant of Si$_3$N$_4$ ceramics, respectively. Theoretical results have shown that the order of magnitude of resonant frequency ω_0 is around 10 eV ($\sim 10^{15}$ Hz) [59, 60] which is considerably larger than the tested frequency ($\sim 10^{10}$ Hz). Combining with Eq. (4), the real permittivity increases slightly with frequency increase, which is closely coincident with the experimental results. Furthermore, taking the effect of temperature into consideration, N and η should follow:

$$N \propto \exp\left(-E_a/RT\right) \tag{7}$$

$$\eta \propto \exp\left(-E_b/RT\right) \tag{8}$$

where E_a and E_b are the activation energy of electrons and lattice, respectively. The dependence of real permittivity of Si$_3$N$_4$ ceramics on temperature at three representative frequencies and the best fitting diagram according to Eqs. (6)–(8) are shown by solid lines in **Figure 9**.

It can be clearly seen that the dielectric constant gradually increases as temperature increased, starting from room temperature to 800°C, and results show that the real permittivity is well distributed on the predicted curves with coefficient of determination (R^2) ranging from 0.91 to 0.93. The characteristic parameters fitted from the temperature dependence of permittivity at three representative frequencies by the Trust-Region algorithm are also listed in **Figure 8**. The activation energy of electrons E_a is distributed between 15.46 and 17.49 KJ/mol, while the activation energy of
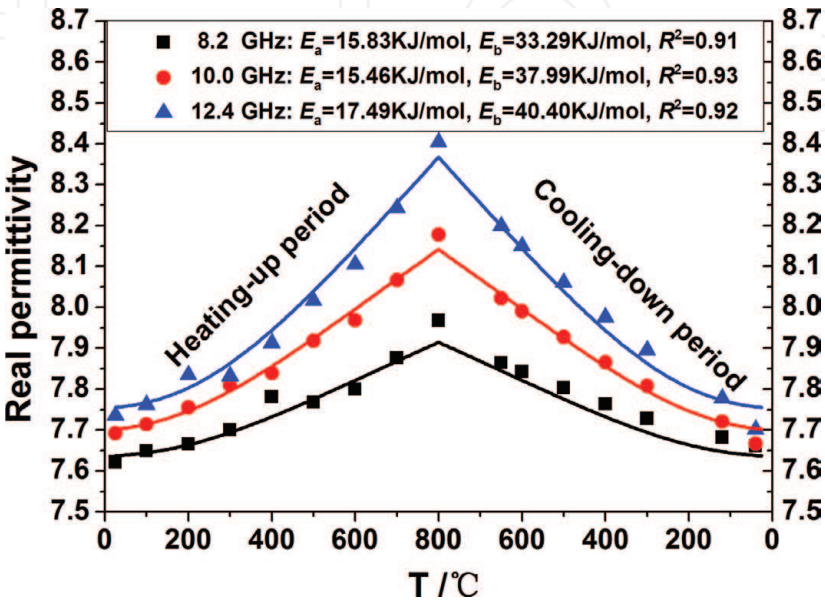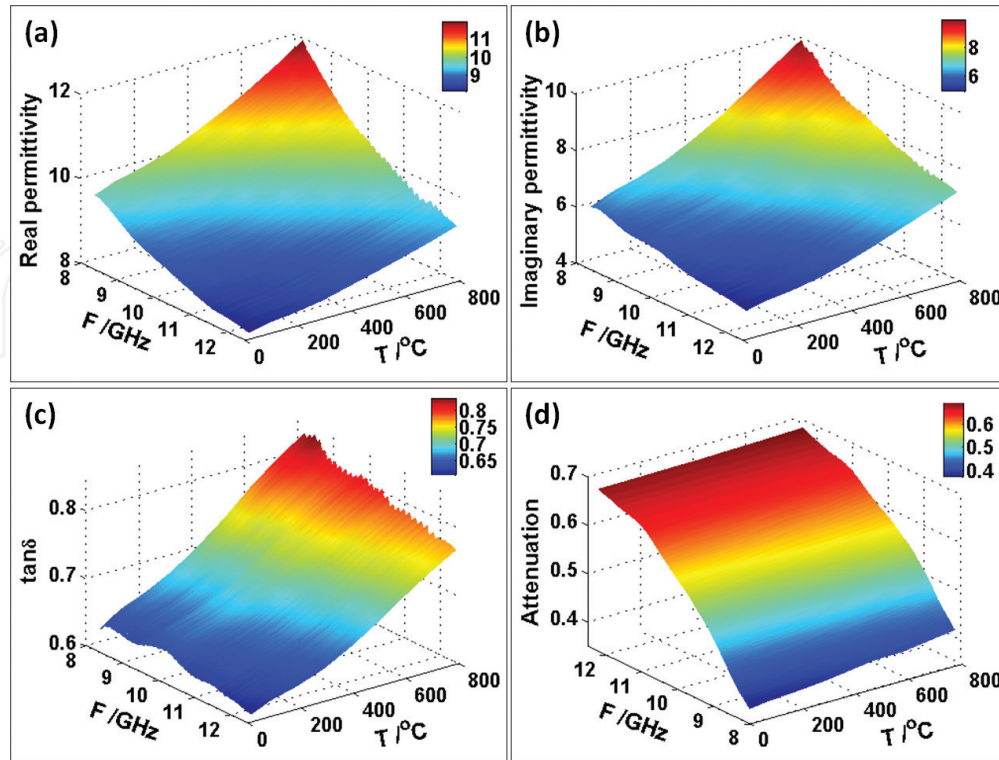

Figure 9.
Dependences of real permittivity of Si$_3$N$_4$ ceramics on temperature (reprinted with permission from Ref. [48]).

lattice E_b is distributed between 33.29 and 40.40 KJ/mol. The activation energy of electronic E_a is less than that of lattice E_b, which is mainly attributed to the binding force between the electrons and nucleus being lower than the covalent bonding force of lattice. Another important feature to be noticed is that the real permittivity of Si_3N_4 ceramics shows symmetrical features between the heating-up and cooling-down periods. The excellent thermo-stability of dielectric properties of Si_3N_4 ceramics has established the foundation for high-temperature radar absorbing materials.

3.4 High-temperature dielectric behaviors of multilayer C_f/Si_3N_4 composites

The evolution of ε' and ε'' for multilayer C_f/Si_3N_4 composites with temperature and frequency is illustrated in **Figure 10(a)** and **(b)**, respectively. It can be clearly seen that both ε' and ε'' of C_f/Si_3N_4 composites are enhanced with temperature. Similar phenomenon was also observed in other microwave-absorbing/shielding materials [24–26, 61–63]. Besides, as shown in **Figure 10(c)**, the loss tangent of C_f/Si_3N_4 composites remains higher than 0.6 over X-band and increases with increase in temperature. After comparison with low-loss β-SiC [64] as well as Si_3N_4, it is fairly clear that short carbon fibers are dominantly responsible for the frequency and temperature-dependent permittivity of C_f/Si_3N_4 composites. This is attributed to the unique microstructure (named skin-core structure), which was confirmed from transmission electron microscope analysis and selected-area electron-diffraction patterns previously [65, 66]. As illustrated in **Figure 11**, the core region consists of graphitic basal planes with random orientation, whereas graphitic basal planes are parallel to the fiber axis in the skin region [66, 67]. Therefore, electron migration behaviors both within and between graphitic basal planes inside carbon fibers would lead to electric charge accumulation at interfaces between carbon fibers and Si_3N_4 matrix (usually referred to as space charge polarization) when exposed to electromagnetic field. Furthermore, this space charge polarization is supposed to be

Figure 10.
Three-dimensional plots of dielectric properties of C_f/Si_3N_4 composites versus frequency and temperature: (a) real part, (b) imaginary part, (c) loss tangent, and (d) attenuation coefficient (reprinted with permission from Ref. [39]).
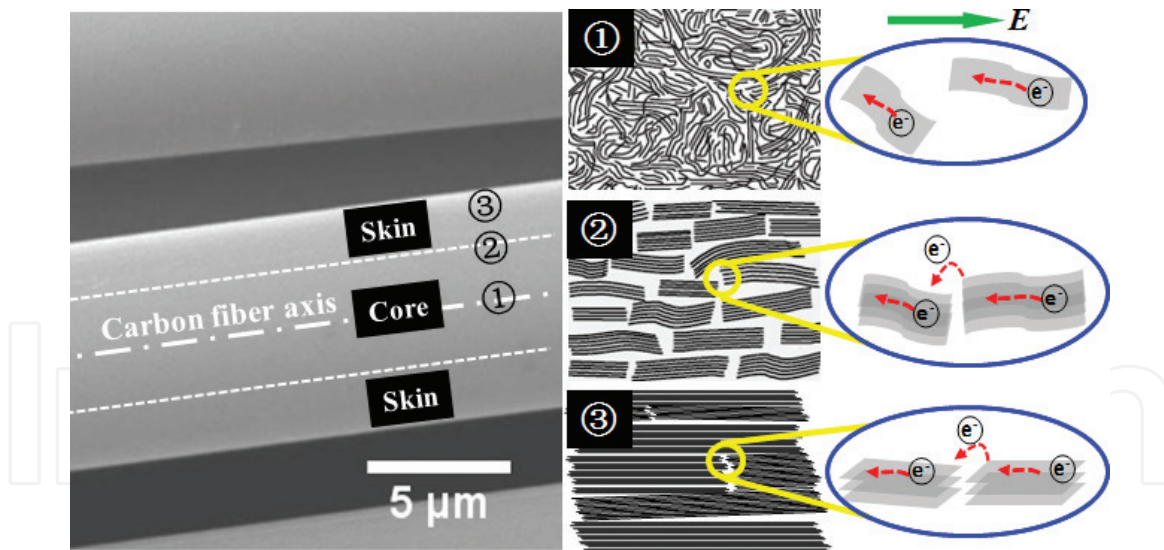
Figure 11.
Sketches of microstructure arrangement and electronic motion in carbon fiber (reprinted with permission from Ref. [39]).

enhanced with temperature rise since more and more electrons would be excited, which is in accordance with results in **Figure 10(a)** and **(b)**.

It should also be noted here that the lattice vibration also enhances with temperature rise, corresponding to the enhancement of scattering effect on migration of electrons. Fortunately, the energy of lattice vibration, which is described by phonons, is so small [68] that the scattering effect on electron migration could be neglected reasonably.

Attenuation coefficient is a quantity that characterizes how easily a material can be penetrated by incident microwave. A large attenuation coefficient means that the beam is quickly "attenuated" (weakened) as it passes through the material. The intrinsic attenuation coefficient of multilayer C_f/Si_3N_4 composites along with temperature and frequency derived from S parameters (i.e. $A = 1\text{-}S_{11}{}^2\text{-}S_{21}{}^2$) is illustrated in **Figure 10(d)**. It can be clearly observed that attenuation coefficient of C_f/Si_3N_4 composites enhances continuously with increase in frequency, and reaches a maximum value around 0.7 at 12.4 GHz, which is almost twice as much as that reported for C_f/SiO_2 composites [25]. This superior absorption performance suggests the multilayer C_f/Si_3N_4 composites to be competitive high-temperature microwave-absorbing materials. Another noteworthy phenomenon in **Figure 10(d)** is that the absorption coefficient remains steady in the investigated temperature range regardless of the loss tangent. As discussed previously, the overall absorbing performance results from reflection on the surface and attenuation inside the materials. However, the increasing permittivity means more severe impedance mismatch between air and the absorbing material, corresponding to reduction of penetrated electromagnetic energy. It could be explained by the reduced part of energy, which compensates the enhanced loss tangent, and consequently leads to a relatively steady absorption coefficient of C_f/Si_3N_4 composites with temperature rise.

3.5 Modeling of temperature-dependent dielectric responses for C_f/Si_3N_4 composites

As explicated in Section 3.2, the dielectric responses for multilayer C_f/Si_3N_4 composites have been evaluated experimentally over X-band. Additionally, the corresponding theoretical relationship of complex permittivity versus frequency at room temperature has been successfully established, which could be expressed as:

$$\varepsilon^{'}(\omega) = \frac{c_1}{\omega^2} + c_2 \tag{9}$$

$$\varepsilon^{''}(\omega) = \frac{\omega^2 + c_3}{c_4 \cdot \omega^3 + c_5 \cdot \omega} \tag{10}$$

where ω refers to the angular frequency (i.e., $\omega = 2\pi f$), and c_1, c_2, c_3, c_4, and c_5 are all pre-experimental parameters that are mainly associated with the surface density of short carbon fiber layers and thickness of Si_3N_4 layers. Herein, we first demonstrate this "room-temperature model" is still available at each evaluated temperature coverage up to 800°C or even higher with the help of nonlinear fitting technology. The best fitting curves of experimental data based on Eqs. (9) and (10) are depicted in **Figure 12**.

As expected, the measured results at each evaluated temperature agree quite well with the theoretical curve with coefficient of determination (R^2) above 0.98. These observed results suggest that both $\varepsilon^{'}$ and $\omega\varepsilon^{''}$ of C_f/Si_3N_4 composites are still inversely proportional to the frequency square ω^2 within the temperature range of 25–800°C. However, a universal model coupled with frequency as well as temperature is urgently needed. Actually, a great deal of effort has been made to model frequency dispersive behaviors of permittivity for dielectrics [45]. It is well established that the development of all dielectric relaxation models that came after classical Debye's could be explicated as:

$$\varepsilon = \varepsilon_\infty + \frac{\varepsilon_s - \varepsilon_\infty}{1 + j\omega\tau} \tag{11}$$

where ε_s and ε_∞ are "static" and "infinite frequency" dielectric constants, respectively; j is the imaginary unit (i.e. equals to $\sqrt{-1}$); ω is the angular frequency; and τ is called the relaxation time. However, it is well known that the Debye model is originally developed for spherical polarizable molecules with a single relaxation time and without interaction between them [69]. Nevertheless, the short carbon fibers act as dipoles when exposed to altering electromagnetic fields oscillating in the microwave band, and electromagnetic field around each dipole is supposed to be coupled with that of neighboring dipoles. Furthermore, the relaxation time of chopped carbon fibers is supposed to be distributed over an interval rather than taking a constant value due to the variation of the fibers' length and the
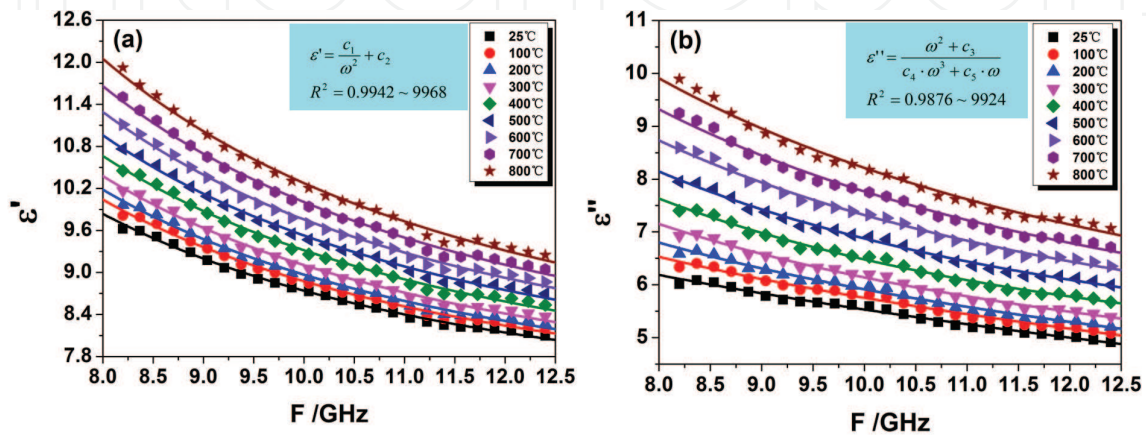
Figure 12.
(a) The real and (b) imaginary parts of permittivity for C_f/Si_3N_4 composites in X-band at the evaluated temperature (reprinted with permission from Ref. [39]).

heterogeneity of fibers' internal structure. This distribution property brings the Debye model (Eq. (11)) into more empirical and given by [25, 26, 70]:

$$\varepsilon = \varepsilon_\infty + \frac{\varepsilon_s - \varepsilon_\infty}{1 + (j\omega\tau)^{1-\alpha}} \tag{12}$$

where α is a parameter which determines the width of the distribution of relaxation time. All parameters in Eq. (12) should be a function of temperature. Substitution of Euler's formula $e^{jx} = \cos(x) + j\sin(x)$ in Eq. (12) yields

$$\varepsilon' = \varepsilon_\infty + \frac{(\varepsilon_s - \varepsilon_\infty) \cdot \left[1 + (\omega\tau)^{1-\alpha} \cdot \sin\frac{\alpha\pi}{2}\right]}{1 + 2(\omega\tau)^{1-\alpha} \cdot \sin\frac{\alpha\pi}{2} + (\omega\tau)^{2(1-\alpha)}} \tag{13}$$

$$\varepsilon'' = \frac{(\varepsilon_s - \varepsilon_\infty) \cdot (\omega\tau)^{1-\alpha} \cdot \cos\frac{\alpha\pi}{2}}{1 + 2(\omega\tau)^{1-\alpha} \cdot \sin\frac{\alpha\pi}{2} + (\omega\tau)^{2(1-\alpha)}} \tag{14}$$

We finally obtain the relationship between ε' and ε'', which could be expressed as

$$\left(\varepsilon' - \frac{\varepsilon_s + \varepsilon_\infty}{2}\right)^2 + \left(\varepsilon'' + \frac{\varepsilon_s + \varepsilon_\infty}{2}\tan\frac{\alpha\pi}{2}\right)^2 = \frac{(\varepsilon_s - \varepsilon_\infty)^2}{4\cos^2\frac{\alpha\pi}{2}} \tag{15}$$

Eq. (15) suggests that the locus of the permittivity in the $(\varepsilon', \varepsilon'')$ complex plane should still be a circular arc with different radius. To put this into perspective, the experimental data are re-plotted in **Figure 13**, in which the best fitted circles based on Eq. (15) are marked as solid curves. As seen, high agreement between the proposed model with experimental data is observed. Besides, the center tends to shift toward greater values of the ε' axis with increase in temperature, suggesting enhanced dielectric strength with temperature according to the Eq. (15). This may be attributed to the Enhanced electron concentration which participated in the polarization process occurs with temperature.

In addition, it is important to highlight some additional details. Firstly, the y-coordinates of fitted circular centers remain so small (~10^{-3}) that Eq. (12) would be reduced to the classical Debye expression. From this point of view, the electronic polarization of short carbon fibers still follows the classic Debye relaxation process. Besides, the effects of temperature and electromagnetic interaction between neighboring short carbon fibers on relaxation time could be neglected reasonably.

Relaxation time also is one of key factors to analyze the dielectric behaviors for composites. After leaving out the effect of α, Eqs. (10) and (11) could be rewritten as follows:

$$\varepsilon' = \frac{1}{\tau} \cdot \frac{\varepsilon''}{\omega} + \varepsilon_\infty \tag{16}$$

It can be clearly seen from Eq. (16) that the real and imaginary parts of permittivity in $(\varepsilon', \varepsilon''/_\omega)$ coordinate should be linear, which is also confirmed in **Figure 13**. What is more, the slope of each line is exactly the inverse of relaxation time τ at a certain temperature evaluated. In this case, we can come to a conclusion that the relaxation time for multilayer C$_f$/Si$_3$N$_4$ composites is weakly dependent on the temperature since the differences between fitted lines are quite modest. For clarity, a detailed plot of τ as a function of temperature is also illustrated as an inset in **Figure 14**. An increase from 216.1 to 250.2 ps has been derived when samples are
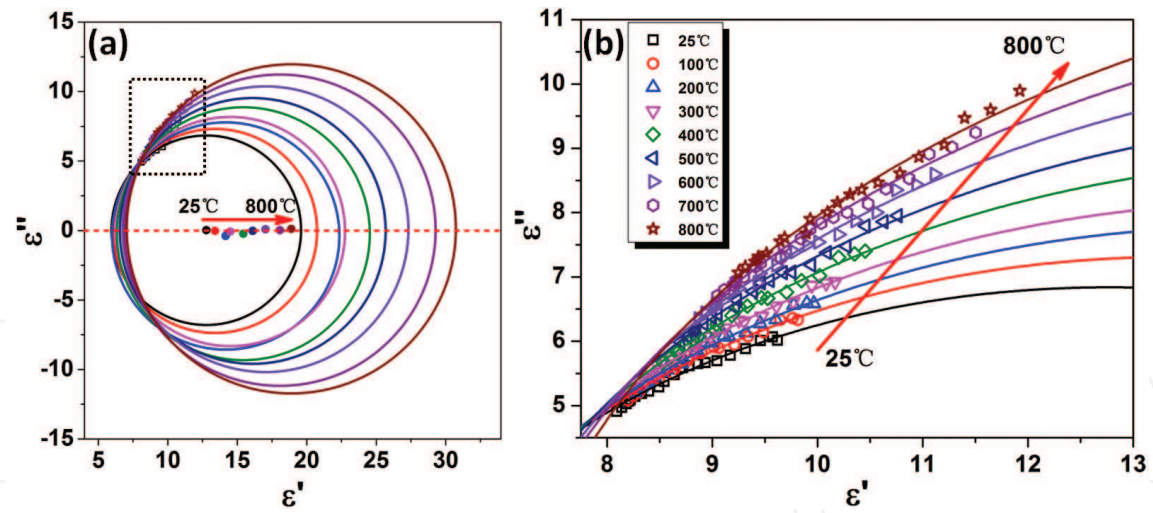
Figure 13.
(a) Argand diagram of C$_f$/Si$_3$N$_4$ composites at different temperature, (b) detailed view for the region marked by black box in (a) (reprinted with permission from Ref. [39]).
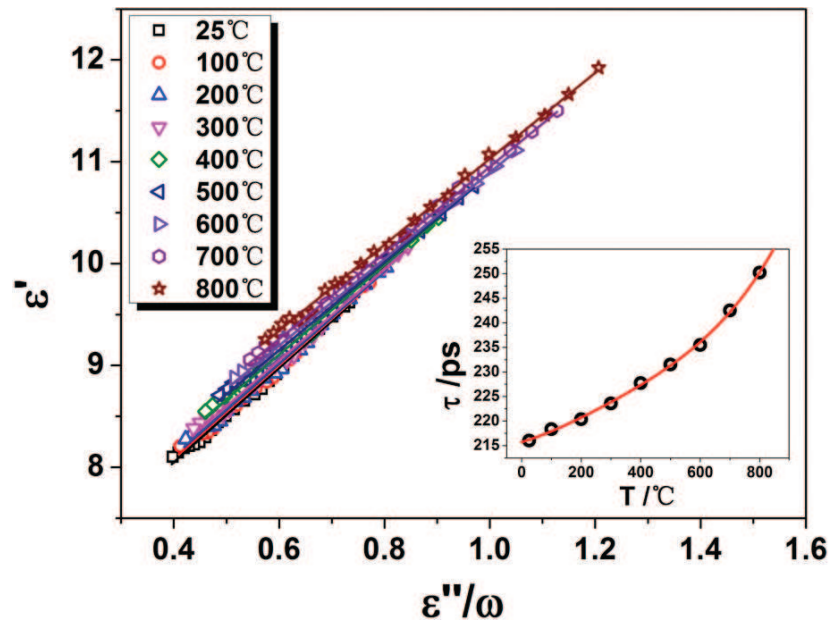
Figure 14.
Plot of ε′ as a function of ε″/ω with an inset of temperature-dependent relaxation time (reprinted with permission from Ref. [39]).

heated from room temperature to 800°C. This gradually increasing trend may be ascribed to the enhancement of scattering effect between electrons for increase both the number and energy of electrons. Furthermore, the relaxation time τ (216.1–250.2 ps) is almost twice as much as a single cycle for time-harmonic electromagnetic wave in X-band ($t_0 = 1/f = 80.65$–121.95 ps). As a result, electronic migration could not keep up with the pace of external alternating electronic field, which leads to continuous decrease of permittivity with frequency increase.

4. Conclusion

In this chapter, microwave dielectric properties of multilayer C$_f$/Si$_3$N$_4$ composites fabricated via gelcasting and pressureless sintering were intensively studied in X-band. Firstly, a strong frequency dependence of the real and imaginary parts of permittivity at room temperature was observed at the X-band. Particularly, an

equivalent RC circuit model concerning the frequency-dependent permittivity of multilayer C$_f$/Si$_3$N$_4$ composites has been established. The predicted results reveal that both ε' and $(\omega \cdot \varepsilon'')$ are inversely proportional to the frequency square, and agree quite well with the measured data. Secondly, high-temperature dielectric behaviors of Si$_3$N$_4$ ceramic show that both permittivity and loss tangent exhibit excellent thermo-stability with temperature coefficient lower than 10^{-3}°C^{-1} within the temperature range of 25–800°C. A revised dielectric relaxation model with Lorentz correction for as-prepared Si$_3$N$_4$ ceramics was established and validated by experimental data. The activation energy of electrons (15.46–17.49 KJ/mol) was demonstrated to be slightly smaller than that of lattice (33.29–40.40 KJ/mol). Finally, the microwave attenuation coefficient of multilayer C$_f$/Si$_3$N$_4$ composites was inclined to be independent of temperature, and a maximum value of 0.7 could be achieved. The obvious positive temperature coefficient characteristic for permittivity is mainly attributed to the enhancement of electric polarization and relaxation of electron migration for graphitic basal planes of short carbon fibers. In addition to the fact that the room-temperature model concerning frequency-dependent permittivity is still available when extended into the full range of temperature coverage up to 800°C, an empirical equation with respect to temperature-dependent permittivity of multilayer C$_f$/Si$_3$N$_4$ composites has been established. It is concluded that the measured complex permittivity of multilayer C$_f$/Si$_3$N$_4$ composites is well distributed on circular arcs with centers actually kept around the real (ε') axis in (ε',ε'') complex plane. Furthermore, the relaxation time as a function of temperature also has been derived. Results suggest that the relaxation time for multilayer C$_f$/Si$_3$N$_4$ composites increases from 216.1 to 250.2 ps when heated from room temperature to 800°C, and is almost twice as much as a single cycle for electromagnetic wave in X-band which leads to continuous decrease in permittivity with frequency increase. These findings point to important guidelines for analyzing high-temperature dielectric behaviors and revealing fundamental mechanisms for carbon fiber functionalized composites including but not limited to C$_f$/Si$_3$N$_4$ composites.

Acknowledgements

Conflict of interest

The authors declared that they have no conflicts of interest to this work.

Author details

Heng Luo[1,2]*, Lianwen Deng[1] and Peng Xiao[2]

1 School of Physics and Electronics, Central South University, Changsha, China

2 State Key Laboratory of Powder Metallurgy, Central South University, Changsha, China

*Address all correspondence to: luohengcsu@csu.edu.cn

IntechOpen

References

[1] Mohan RR, Varma SJ, Sankaran J. Impressive electromagnetic shielding effects exhibited by highly ordered, micrometer thick polyaniline films. Applied Physics Letters. 2016;**108**(15):154101. DOI: 10.1063/1.4945791

[2] Zhao Y-T et al. Transparent electromagnetic shielding enclosure with CVD graphene. Applied Physics Letters. 2016;**109**(10):103507. DOI: 10.1063/1.4962474

[3] Zeng Z et al. Thin and flexible multi-walled carbon nanotube/ waterborne polyurethane composites with high-performance electromagnetic interference shielding. Carbon. 2016;**96**:768-777. DOI: 10.1016/j.carbon.2015.10.004

[4] Wen B et al. Reduced graphene oxides: Light-weight and high-efficiency electromagnetic interference shielding at elevated temperatures (Adv. Mater. 21/2014). Advanced Materials. 2014;**26**(21):3357-3357. DOI: 10.1002/adma.201470138

[5] Shahzad F et al. Electromagnetic interference shielding with 2D transition metal carbides (MXenes). Science. 2016;**353**(6304):1137-1140. DOI: 10.1126/science.aag2421

[6] Zhang Y et al. Additive manufacturing of carbon nanotube-photopolymer composite radar absorbing materials. Polymer Composites. 2016. DOI: 10.1002/pc.24117

[7] Hayashida K, Matsuoka Y. Electromagnetic interference shielding properties of polymer-grafted carbon nanotube composites with high electrical resistance. Carbon. 2015;**85**:363-371. DOI: 10.1016/j.carbon.2015.01.006

[8] Li N et al. Electromagnetic interference (EMI) shielding of single-walled carbon nanotube epoxy composites. Nano Letters. 2006;**6**(6):1141-1145. DOI: 10.1021/nl0602589

[9] Micheli D et al. X-Band microwave characterization of carbon-based nanocomposite material, absorption capability comparison and RAS design simulation. Composites Science and Technology. 2010;**70**(2):400-409. DOI: 10.1016/j.compscitech.2009.11.015

[10] Al-Saleh MH, Sundararaj U. A review of vapor grown carbon nanofiber/polymer conductive composites. Carbon. 2009;**47**(1):2-22. DOI: 10.1016/j.carbon.2008.09.039

[11] Han M et al. Hierarchical graphene/SiC nanowire networks in polymer-derived ceramics with enhanced electromagnetic wave absorbing capability. Journal of the European Ceramic Society. 2016;**36**(11):2695-2703. DOI: 10.1016/j.jeurceramsoc.2016.04.003

[12] Huang X et al. A three-dimensional graphene/Fe3O4/carbon microtube of sandwich-type architecture with improved wave absorbing performance. Scripta Materialia. 2016;**120**:107-111. DOI: 10.1016/j.scriptamat.2016.04.025

[13] Olmedo L, Hourquebie P, Jousse F. Microwave absorbing materials based on conducting polymers. Advanced Materials. 1993;**5**(5):373-377. DOI: 10.1002/adma.19930050509

[14] Huang Y et al. The microwave absorption properties of carbon-encapsulated nickel nanoparticles/silicone resin flexible absorbing material. Journal of Alloys and Compounds. 2016;**682**:138-143. DOI: 10.1016/j.jallcom.2016.04.289

[15] Chen Y et al. Enhanced electromagnetic interference shielding efficiency of polystyrene/graphene composites with magnetic Fe_3O_4 nanoparticles. Carbon. 2015;**82**:67-76. DOI: 10.1016/j.carbon.2014.10.031

[16] Al-Saleh MH, Saadeh WH, Sundararaj U. EMI shielding effectiveness of carbon based nanostructured polymeric materials: A comparative study. Carbon. 2013;**60**:146-156. DOI: 10.1016/j.carbon.2013.04.008

[17] Qin F, Brosseau C. A review and analysis of microwave absorption in polymer composites filled with carbonaceous particles. Journal of Applied Physics. 2012;**111**(6):061301. DOI: 10.1063/1.3688435

[18] Chung DDL. Carbon materials for structural self-sensing, electromagnetic shielding and thermal interfacing. Carbon. 2012;**50**(9):3342-3353. DOI: 10.1016/j.carbon.2012.01.031

[19] Liu L, Das A, Megaridis CM. Terahertz shielding of carbon nanomaterials and their composites – A review and applications. Carbon. 2014;**69**:1-16. DOI: 10.1016/j.carbon.2013.12.021

[20] Qin F, Peng H-X. Ferromagnetic microwires enabled multifunctional composite materials. Progress in Materials Science. 2013;**58**(2):183-259. DOI: 10.1016/j.pmatsci.2012.06.001

[21] Yin X et al. Electromagnetic properties of Si–C–N based ceramics and composites. International Materials Reviews. 2014;**59**(6):326-355. DOI: 10.1179/1743280414Y.0000000037

[22] Duan W et al. A review of absorption properties in silicon-based polymer derived ceramics. Journal of the European Ceramic Society. 2016;**36**(15):3681-3689. DOI: 10.1016/j.jeurceramsoc.2016.02.002

[23] Yin X et al. Dielectric, electromagnetic absorption and interference shielding properties of porous yttria-stabilized zirconia/silicon carbide composites. Ceramics International. 2012;**38**(3):2421-2427. DOI: 10.1016/j.ceramint.2011.11.008

[24] Wen B et al. Reduced graphene oxides: Light-weight and high-efficiency electromagnetic interference shielding at elevated temperatures. Advanced Materials. 2014;**26**(21):3484-3489. DOI: 10.1002/adma.201400108

[25] Cao M-S et al. The effects of temperature and frequency on the dielectric properties, electromagnetic interference shielding and microwave-absorption of short carbon fiber/silica composites. Carbon. 2010;**48**(3):788-796. DOI: 10.1016/j.carbon.2009.10.028

[26] Wen B et al. Temperature dependent microwave attenuation behavior for carbon-nanotube/silica composites. Carbon. 2013;**65**:124-139. DOI: 10.1016/j.carbon.2013.07.110

[27] Kong L et al. High-temperature electromagnetic wave absorption properties of $ZnO/ZrSiO_4$ composite ceramics. Journal of the American Ceramic Society. 2013;**96**(7):2211-2217. DOI: 10.1111/jace.12321

[28] Iveković A et al. Current status and prospects of SiCf/SiC for fusion structural applications. Journal of the European Ceramic Society. 2013;**33**(10):1577-1589. DOI: 10.1016/j.jeurceramsoc.2013.02.013

[29] Liu H, Tian H, Cheng H. Dielectric properties of SiC fiber-reinforced SiC matrix composites in the temperature range from 25 to 700°C at frequencies between 8.2 and 18GHz. Journal of Nuclear Materials. 2013;**432**(1-3):57-60. DOI: 10.1016/j.jnucmat.2012.08.026

[30] Tian H, Liu H-T, Cheng H-F. A high-temperature radar absorbing

structure: Design, fabrication, and characterization. Composites Science and Technology. 2014;**90**:202-208. DOI: 10.1016/j.compscitech.2013.11.013

[31] Azarhoushang B, Soltani B, Zahedi A. Laser-assisted grinding of silicon nitride by picosecond laser. The International Journal of Advanced Manufacturing Technology. 2017;**93**(5):2517-2529. DOI: 10.1007/s00170-017-0440-9

[32] Xu Y et al. Shear-thinning behavior of the CaO-SiO$_2$-CaF$_2$-Si$_3$N$_4$ system mold flux and its practical application. International Journal of Minerals, Metallurgy, and Materials. 2017;**24**(10):1096-1103. DOI: 10.1007/s12613-017-1500-8

[33] Zuo K-H, Zeng Y-P, Jiang D-L. The mechanical and dielectric properties of Si$_3$N$_4$-based sandwich ceramics. Materials & Design. 2012;**35**:770-773. DOI: 10.1016/j.matdes.2011.09.019

[34] Yang J, Yu J, Huang Y. Recent developments in gelcasting of ceramics. Journal of the European Ceramic Society. 2011;**31**(14):2569-2591. DOI: 10.1016/j.jeurceramsoc.2010.12.035

[35] Luo H et al. Dielectric properties of Cf–Si3N4 sandwich composites prepared by gelcasting. Ceramics International. 2014;**40**(6):8253-8259. DOI: 10.1016/j.ceramint.2014.01.023

[36] Bocanegra-Bernal MH, Matovic B. Mechanical properties of silicon nitride-based ceramics and its use in structural applications at high temperatures. Materials Science and Engineering A. 2010;**527**(6):1314-1338. DOI: 10.1016/j.msea.2009.09.064

[37] Dambatta YS et al. Ultrasonic assisted grinding of advanced materials for biomedical and aerospace applications—a review. The International Journal of Advanced Manufacturing Technology.

2017;**92**(9):3825-3858. DOI: 10.1007/s00170-017-0316-z

[38] Tatli Z, Thompson DP. Low temperature densification of silicon nitride materials. Journal of the European Ceramic Society. 2007;**27**(2-3):791-795. DOI: 10.1016/j.jeurceramsoc.2006.04.010

[39] Luo H et al. Modeling for high-temperature dielectric behavior of multilayer Cf/Si3N4 composites in X-band. Journal of the European Ceramic Society. 2017;**37**(5):1961-1968. DOI: 10.1016/j.jeurceramsoc.2016.12.028

[40] Peng C-H, Chen PS, Chang C-C. High-temperature microwave bilayer absorber based on lithium aluminum silicate/lithium aluminum silicate-SiC composite. Ceramics International. 2014;**40**(1 Part A):47-55. DOI: 10.1016/j.ceramint.2013.05.101

[41] Yuan J et al. High dielectric loss and microwave absorption behavior of multiferroic BiFeO$_3$ ceramic. Ceramics International. 2013;**39**(6):7241-7246. DOI: 10.1016/j.ceramint.2013.01.068

[42] Qing YC et al. Microwave absorbing ceramic coatings with multi-walled carbon nanotubes and ceramic powder by polymer pyrolysis route. Composites Science and Technology. 2013;**89**:10-14. DOI: 10.1016/j.compscitech.2013.09.007

[43] Liu H, Cheng H, Tian H. Design, preparation and microwave absorbing properties of resin matrix composites reinforced by SiC fibers with different electrical properties. Materials Science and Engineering B. 2014;**179**:17-24. DOI: 10.1016/j.mseb.2013.09.019

[44] Chen M et al. Gradient multilayer structural design of CNTs/SiO$_2$ composites for improving microwave absorbing properties. Materials & Design. 2011;**32**(5):3013-3016. DOI: 10.1016/j.matdes.2010.12.043

[45] Luo H, Xiao P, Hong W. Dielectric behavior of laminate-structure Cf/Si_3N_4 composites in X-band. Applied Physics Letters. 2014;**105**(17):172903. DOI: 10.1063/1.4900932

[46] Cui TJ, Smith D, Liu R. Metamaterials: Theory, Design, and Applications. 233 Spring Street, New York, USA Springer Publishing Company, Incorporated; 2009. p. 368

[47] Liu Y, Zhang X. Metamaterials: A new frontier of science and technology. Chemical Society Reviews. 2011;**40**(5):2494-2507. DOI: 10.1039/C0CS00184H

[48] Shao S et al. Effect of temperature on dielectric response in X-band of silicon nitride ceramics prepared by gelcasting. AIP Advances. 2018;**8**(7):075127. DOI: 10.1063/1.5033965

[49] Amirat Y, Shelukhin V. Homogenization of time harmonic Maxwell equations and the frequency dispersion effect. Journal de Mathématiques Pures et Appliquées. 2011;**95**(4):420-443. DOI: 10.1016/j.matpur.2010.10.007

[50] Haijun Z et al. Complex permittivity, permeability, and microwave absorption of Zn- and Ti-substituted barium ferrite by citrate sol–gel process. Materials Science and Engineering B. 2002;**96**(3):289-295. DOI: 10.1016/S0921-5107(02)00381-1

[51] Joshi A, Kumar S, Verma NK. Study of dispersion, absorption and permittivity of an synthetic insulation paper—with change in frequency and thermal aging. NDT & E International. 2006;**39**(1):19-21. DOI: 10.1016/j.ndteint.2005.05.004

[52] Kamenetsky FM. Frequency dispersion of rock properties in equations of electromagnetics. Journal of Applied Geophysics. 2011;**74**(4):185-193. DOI: 10.1016/j.jappgeo.2011.04.004

[53] Razzitte AC, Fano WG, Jacobo SE. Electrical permittivity of Ni and NiZn ferrite–polymer composites. Physica B: Condensed Matter. 2004;**354**(1-4):228-231. DOI: 10.1016/j.physb.2004.09.054

[54] Rica RA, Jiménez ML, Delgado AV. Electric permittivity of concentrated suspensions of elongated goethite particles. Journal of Colloid and Interface Science. 2010;**343**(2):564-573. DOI: 10.1016/j.jcis.2009.11.063

[55] Tan YQ et al. Giant dielectric-permittivity property and relevant mechanism of $Bi_{2/3}Cu_3Ti_4O_{12}$ ceramics. Materials Chemistry and Physics. 2010;**124**(2-3):1100-1104. DOI: 10.1016/j.matchemphys.2010.08.041

[56] Moysés Araújo C et al. Electrical resistivity, MNM transition and band-gap narrowing of cubic GaN: Si. Microelectronics Journal. 2002;**33**(4):365-369. DOI: 10.1016/S0026-2692(01)00133-1

[57] Fernandez JRL et al. Electrical resistivity and band-gap shift of Si-doped GaN and metal-nonmetal transition in cubic GaN, InN and AlN systems. Journal of Crystal Growth. 2001;**231**(3):420-427. DOI: 10.1016/S0022-0248(01)01473-7

[58] Schuurmans FJP, Vries Pd, Lagendijk A. Local-field effects on spontaneous emission of impurity atoms in homogeneous dielectrics. Physics Letters A. 2000;**264**(6):472-477. DOI: 10.1016/S0375-9601(99)00855-5

[59] Hao Wang YC, Kaneta Y, Iwata S. First-principles investigation of the structural, electronic and optical properties of olivine-Si3N4 and olivine-Ge3N4. Journal of Physics: Condensed Matter. 2006;**18**(47):10663-10676. DOI: 10.1088/0953-8984/18/47/012

[60] Xu M et al. Theoretical prediction of electronic structures and optical properties of Y-doped γ-Si3N4. Physica B: Condensed Matter. 2008;**403** (13-16):2515-2520. DOI: 10.1016/j. physb.2008.01.042

[61] Yang H-J et al. Silicon carbide powders: Temperature-dependent dielectric properties and enhanced microwave absorption at gigahertz range. Solid State Communications. 2013;**163**:1-6. DOI: 10.1016/j. ssc.2013.03.004

[62] Wang H et al. High temperature electromagnetic and microwave absorbing properties of polyimide/ multi-walled carbon nanotubes nancomposites. Chemical Physics Letters. 2015;**633**:223-228. DOI: 10.1016/j.cplett.2015.05.048

[63] Dou Y-K et al. The enhanced polarization relaxation and excellent high-temperature dielectric properties of N-doped SiC. Applied Physics Letters. 2014;**104**(5):052102. DOI: 10.1063/1.4864062

[64] Liu Y et al. Transmission electron microscopy study of the microstructure of unidirectional C/C composites fabricated by catalytic chemical vapor infiltration. Carbon. 2013;**51**:381-389. DOI: 10.1016/j. carbon.2012.08.070

[65] Koziel S, Bekasiewicz A. Multi-objective optimization of expensive electromagnetic simulation models. Applied Soft Computing. 2016;**47**: 332-342. DOI: 10.1016/j. asoc.2016.05.033

[66] Zhou G et al. Microstructure difference between core and skin of T700 carbon fibers in heat-treated carbon/carbon composites. Carbon. 2011;**49**(9):2883-2892. DOI: 10.1016/j. carbon.2011.02.025

[67] Qin X et al. A comparison of the effect of graphitization on

microstructures and properties of polyacrylonitrile and mesophase pitch-based carbon fibers. Carbon. 2012;**50**(12):4459-4469. DOI: 10.1016/j. carbon.2012.05.024

[68] Cai Y et al. First-principles study of vibrational and dielectric properties of β-Si3N4. Physical Review B. 2006;**74**(17):174301. DOI: 10.1103/ PhysRevB.74.174301

[69] Kirkwood JG, Fuoss RM. Anomalous dispersion and dielectric loss in polar polymers. The Journal of Chemical Physics. 1941;**9**(4):329-340. DOI: 10.1063/1.1750905

[70] Cole KS, Cole RH. Dispersion and absorption in dielectrics I. Alternating current characteristics. The Journal of Chemical Physics. 1941;**9**(4):341-351. DOI: 10.1063/1.1750906